The International Journal of Advanced Manufacturing Technology (2023) 124:3201–3215
https://doi.org/10.1007/s00170-022-10513-8

ORIGINAL ARTICLE

Analytical prediction of cutting forces in cylindrical turning of 304 stainless steel using unequal division shear zone theory

Binglin Li[1,2] · **Rui Zhang**[1]

Received: 1 March 2022 / Accepted: 9 November 2022 / Published online: 1 December 2022

Abstract

In order to establish a more accurate prediction model of turning forces, this paper proposed an analytical model for cylindrical turning with the consideration of the effect of the main cutting edge angle and the nose radius. Meanwhile, the unequal division shear zone theory in orthogonal free cutting is extended and applied to the oblique non-free cutting in the interaction between the chip units. To take into account the real tool nose geometry, the tool nose involved in the cutting is discretized into a series of cutting edge units. The geometrical parameters associated with the cutting edge units are analysed by using the coordinate transformation approach. Then, the improved oblique cutting model is applied to each cutting edge unit to acquire the component forces along the tool rake face. Finally, the resultant cutting forces in the turning process are calculated by the numerical integration method. To verify the effectiveness of the proposed model, the turning force experiment of 304 stainless steel was carried out by changing the cutting conditions, the main cutting edge angle, and the nose radius. Through the comparative analysis between the measured results and the calculation values of the proposed model, it was found that the analytical prediction of cutting force is in good agreement with the experiment.

Keywords Oblique cutting · Non-free cutting · Unequal division shear zone theory · Cutting edge discretization · Cutting force prediction

1 Introduction

Through the accurate prediction of cutting force, the tool and machining parameters can be reasonably selected to improve cutting performance. Many researchers around the world have also done a lot of research on oblique cutting, because the majority of metal machining is non-free oblique cutting. At present, although most of the research is focused on the cutting force prediction of orthogonal free cutting, in which the cutting direction is performed along one straight cutting edge, non-free cutting, in which both primary and minor cutting edges are involved, is most widely used such as cylindrical turning in practice. The cutting conditions, the nose radius, and the main cutting edge angle also affect the cutting force in turning; therefore, comprehensive consideration of these factors is essential to accurately predict cutting forces. Besides, the dead metal zone also has major effect on cutting force and cutting performance in micro-machining [1, 2].

Cylindrical turning, one of the commonest processes in manufacturing components, is widely used in automotive, aerospace, and so on. It is a typical non-free cutting operation whose chip deformation process is very complex. The calculation of cutting forces in turning is roughly divided into three methods: empirical, analytical, and numerical models. Parakkal et al. [3] developed a relatively simple mechanistic model to predict cutting forces for grooved tool in oblique cutting, which considered the effect of the tool edge radius. This model was used to investigate the effects of cutting conditions and grooved parameters on the cutting forces. Kone et al. [4]. identified empirical cutting force equations; the chip flow angle of groove coated tool cutting 304L austenitic steel under dry cutting condition is deduced. Venkatarao [5, 6] proposed a power consumption optimization-base strategy couple with 3D FEM simulation to reduce power consumption in micro-machining, the optimal value of process

✉ Binglin Li
libinglin@swpu.edu.cn

[1] School of Mechatronic Engineering, Southwest Petroleum University, Chengdu, China

[2] School of Mechanical Science and Engineering, Huazhong University of Science and Technology, Wuhan, China

parameters is obtained for minimum cutting force, and a power consumption model was developed in terms of cutting force directions in ultrasonic vibration helical milling. Colwell [7] proposed the equivalent cutting edge that is used to replace the real cutting edge with an imaginary straight line in the tool rake face and assumed that the equivalent cutting edge is perpendicular to the chip flow direction. However, the chip flow direction defined above is not suited for cylindrical turning due to the nose radius. Hu et al. [8] extended Colwell's concept of equivalent cutting edge to the case of non-zero inclination angle. Kushima and Minato [9] divided the cutting edge into many small units and supposed that the component chip flow direction of each unit is perpendicular to the component cutting edge, and then the resultant chip flow direction is obtained by vectorial sum of the component chip flow directions. Young et al. [10] regarded the chip as many independent chip units and assumed that the thickness and direction of undeformed chip part of each unit are variable. The equivalent cutting edge is a straight line perpendicular to the direction of friction and can be obtained by calculating the resultant force per unit friction. Similarly, Wang et al. [11]. extended Young's method to the tool nose with non-zero rake and inclination angle and evaluated cutting force through numerical integration. Endres et al. [12]. introduced a nonlinear relationship among the unit friction, cutting force, and the chip thickness by considering the size effect of rounded edge on the tool nose. Khlifi et al. [13]. applied an equivalent tool geometry method to induce the same cutting force components as the real tool while taking into account the radius of the tool nose and edge. In addition to estimating the tool flank and crater wear, this method can also predict cutting force components in turning.

In the primary shear zone, Merchant [14] proposed a single shear plane analytical model. The shear angle was obtained by the minimum energy theory; many analytical models were then proposed for the modeling of orthogonal cutting process, such as the classical parallel-sided shear zone theory proposed by Oxley [15], which supposed that the primary shear zone is equally divided by the primary shear plane. However, Li et al. [16] established the unequal division shear zone theory by observing the strain rate distribution in the primary shear zone is inconsistent, the analytical results showed that the unequal division shear zone theory has acceptable accuracy. In subsequent research, this model is widely used to predict the cutting force and chip flow direction and to identify material constitutive equation. In addition, the existence of the rounded nose and the main cutting edge angle makes the cutting mechanism more complicated. Simultaneously, they have a significant influence on the geometry of the undeformed chip area, cutting forces, chip geometry, heat generation, and tool wear during turning. Redetzky et al. [17] divided the cutting edge into many trapezoidal units that are perpendicular to the component edge and calculated the cutting force of each discrete unit through unit cutting force, unit edge force, and unit lateral force. Hagiwara et al. [18] developed the hybrid model by Redetzky et al. [17] to predict the chip side-flow angle for complex grooved tool inserts in contour turning operations by applying the effective cutting conditions and tool geometry. Armarego et al. [19]. put forward to the generalized cutting edge concept to replace the rounded edge of tool nose. Storch et al. [20] investigated the unit force distribution on the rounded edge for free cutting and found that both the tool nose and the main cutting edge affect the machined surface quality and chip formation process. Fang [21] developed an improved oblique cutting model different from traditional model by considering the two cases where the tool main cutting edge angle is not equal to 90° and the influence of the tool feed velocity on the resultant cutting velocity is not ignored. Molinari et al. [22] established a new thermo-mechanical model of oblique cutting to take into account the real cutting edge geometry; the rounded nose is discretized into a set of cutting edge units to obtain the component cutting force and temperature distribution along the rake face, but their oblique model is based on the inertia item, mainly suitable for adiabatic shear process in high-speech machining. Budak et al. [23] proposed a thermo-mechanical model that considered both the sticking and sliding contact on rake face, and applied this model to obtained the local forces acting on each element by dividing the nose of the turning into small elements. Abdellaoui et al. [24] also analysed the effects of tool nose radius and established a thermo-mechanical model, which allows predicting cutting force components and thermo-mechanical parameters.

In conclusion, the existing turning force prediction model mainly apply the single shear plane theory and the parallel shear zone theory in the primary shear zone. In such case, these models cannot accurately describe the real plastic deformation state and stress–strain relationship of the primary shear zone. In this paper, a novel turning force prediction model based on unequal shear theory is presented for cylindrical turning, considering the influence of the tool nose radius and the main cutting edge angle on cutting force.

In this present work, the oblique cutting theory based on the unequal division shear zone theory investigated by Li et al. [16, 25], and combined with the tool discretization approach of Molinari and Moufki [22], is developed to predict the cutting forces in turning of 304 stainless steel. This paper is organized as follows. Section 2 presents the analytical modeling of non-free oblique cutting with geometrical characterization and governing equations. The unequal shear theory and material constitutive equation are described in Sect. 3. In Sect. 4, the discretization of the tool cutting edge and the component geometry of each cutting edge unit are described. The component and resultant cutting force calculation are detailed in Sect. 5. The turning experiments for

304 stainless steel were conducted, and the effect of cutting parameters on cutting force is also discussed in Sect. 6. Finally, some conclusions are provided in Sect. 7.

2 Characteristics of the improved oblique cutting

To study the turning process, an analytical model of oblique cutting of the unequal division shear zone theory is developed for the case that the tool cutting edge angle relative to the main cutting edge is not equal to 90°, namely, the feed rate f_r is not equal to the undeformed chip thickness t. In view of this, Fang [21] also proposed an improved method for the oblique cutting model and applied it to chip control experiment. Figure 1 illustrates the process of improved oblique cutting.

In this model, where t, a_w, and φ_r are undeformed chip thickness, cutting width, and lead angle (complementary angle of the main cutting edge angle κ_r), respectively. The cutting depth a_p, feed rate f_r, cutting velocity V, normal rake angle γ_n, and inclination angle λ_s are known, and the geometric relations of these parameters are shown in Fig. 2. Some planes that can be used to determine the location of the cutting edges, rake face, and flank face are defined.

- The reference plane P_r
- The working plane P_f
- The back plane P_p
- The cutting plane P_s
- The orthogonal plane P_o
- The normal plane P_n
- The shear plane P_{sh}
- The equivalent plane P_e

As shown in Figs. 1 and 2, to calculate the relationships of geometry, motion, and force in the improved oblique cutting model, a series of coordinate systems are defined.

- Frame ($\boldsymbol{x}_a$, $\boldsymbol{y}_a$, $\boldsymbol{z}_a$), $\boldsymbol{x}_a$ is parallel to the cutting velocity direction, $\boldsymbol{z}_a$ is parallel to the feed direction, ($\boldsymbol{x}_a$, $\boldsymbol{y}_a$) is the back plane P_p, ($\boldsymbol{y}_a$, $\boldsymbol{z}_a$) is the reference plane P_r, ($\boldsymbol{x}_a$, $\boldsymbol{z}_a$) is the working plane P_f.
- Frame ($\boldsymbol{x}_o$, $\boldsymbol{y}_o$, $\boldsymbol{z}_o$)
- Frame ($\boldsymbol{x}_n$, $\boldsymbol{y}_n$, $\boldsymbol{z}_n$)
- Frame ($\boldsymbol{x}_r$, $\boldsymbol{y}_r$, $\boldsymbol{z}_r$)
- Frame ($\boldsymbol{x}$, $\boldsymbol{y}$, $\boldsymbol{z}$)
- Frame ($\boldsymbol{x}_c$, $\boldsymbol{y}_c$, $\boldsymbol{z}_c$)
- Frame ($\boldsymbol{x}_s$, $\boldsymbol{y}_s$, $\boldsymbol{z}_s$)
- Frame ($\boldsymbol{x}_e$, $\boldsymbol{y}_e$, $\boldsymbol{z}_e$)

The eight frames can be related by rotation transformation, as shown in Fig. 3. Take for example, ($\boldsymbol{x}_o$, $\boldsymbol{y}_o$, $\boldsymbol{z}_o$) is obtained by the rotation of angle -φ_r of the frame ($\boldsymbol{x}_a$, $\boldsymbol{y}_a$, $\boldsymbol{z}_a$) around the $\boldsymbol{x}_a$ axis. It can be expressed as the following form:

$$(\mathbf{x}_a, \mathbf{y}_a, \mathbf{z}_a) \xrightarrow{\mathbf{R}(x_a, -\varphi_r)} (\mathbf{x}_o, \mathbf{y}_o, \mathbf{z}_o)$$

The rest of the frames can also be given by the above method; ϕ_n is the normal shear angle, η_c is the chip flow

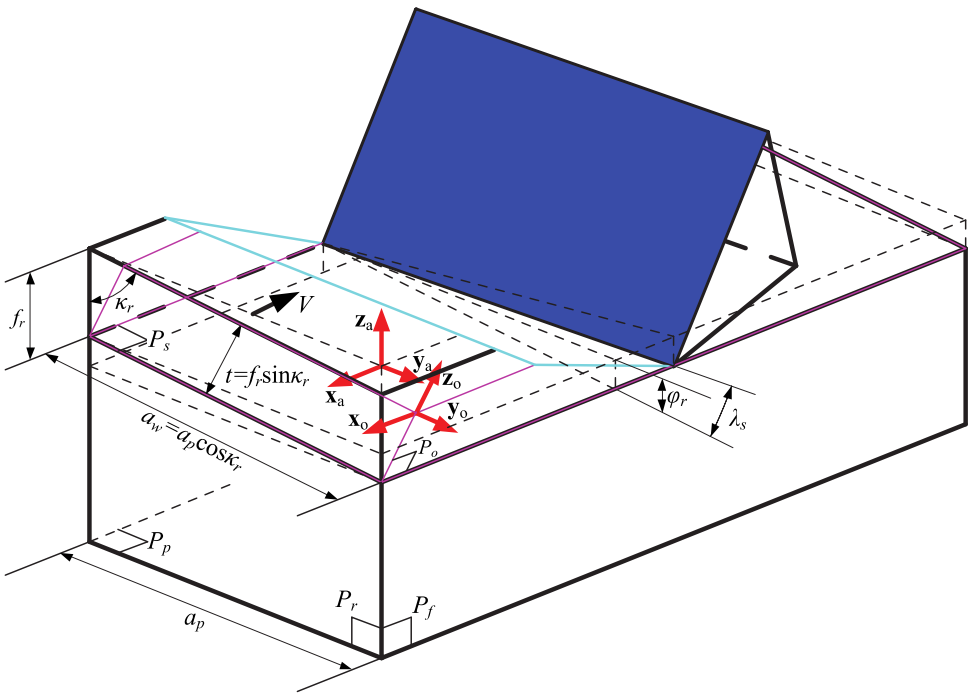

Fig. 1 The improved oblique cutting process

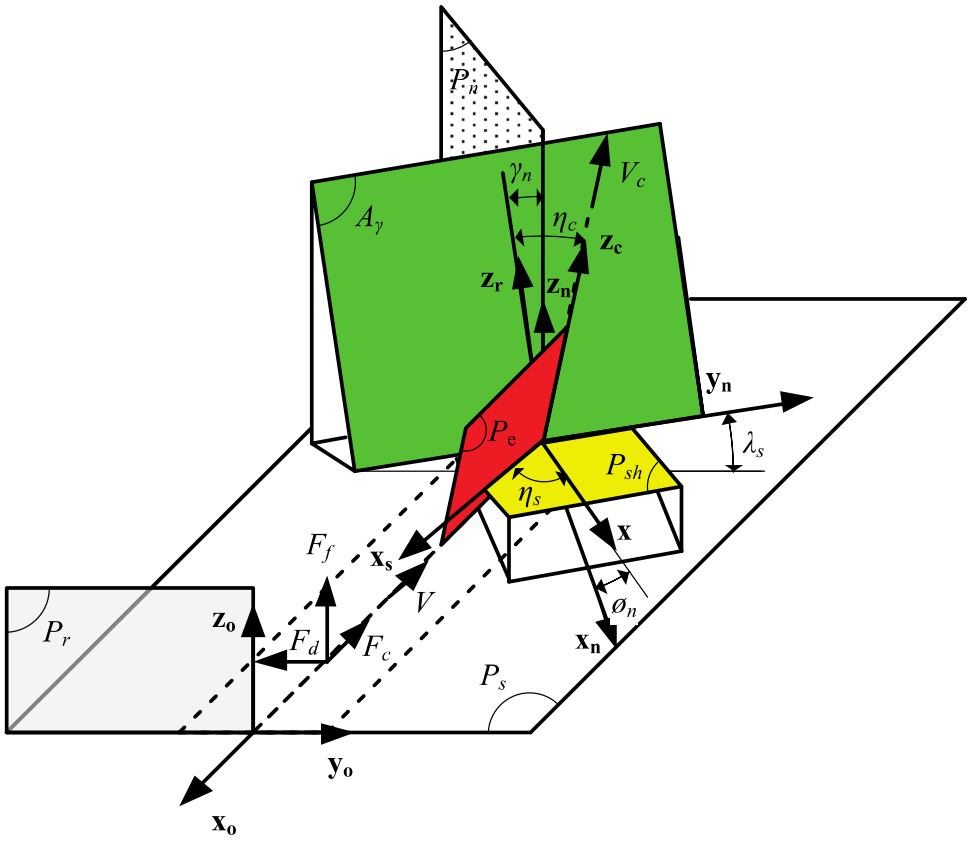

Fig. 2 The geometrical relationship of oblique cutting

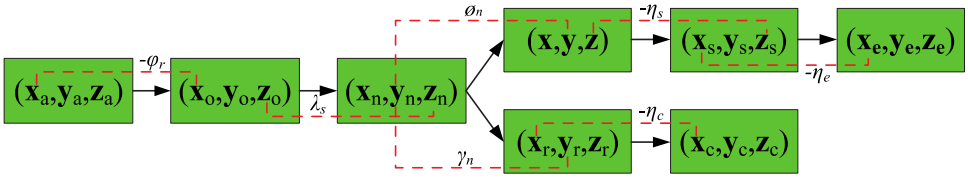

Fig. 3 The rotation transformation relationships between the coordinate systems

angle, η_s is the shear flow angle, and η_e is the equivalent plane angle. To locate the equivalent plane of each discrete edge unit, of which k is used to represent the number, the shear flow angle and the equivalent plane angle are taken by the following expression [22].

$$tan\ \eta_e^k = \frac{\tan\ \eta_c^k \cos\ \eta_s^k + \sin(\phi_n^k - \gamma_n^k) \sin\ \eta_s^k}{\cos(\phi_n^k - \gamma_n^k)} \tag{1}$$

$$tan\ \eta_s^k = \frac{\tan\ \lambda_s^k \cos(\phi_n^k - \gamma_n^k) - \tan\ \eta_c^k \sin\ \phi_n^k}{\cos \gamma_n^k} \tag{2}$$

Since the chip flow angle is affected by the non-free chip in turning, the chip flow angle η_c formula of free oblique cutting which was proposed by Moufki and Molinari [26] or others no longer suitable for no-free oblique cutting. The chip velocity can be calculated as:

$$V_c^k = \frac{V \cos\ \lambda_s^k \sin \phi_n^k}{\cos\ \eta_c^k \cos(\phi_n^k - \gamma_n^k)} \tag{3}$$

The normal shear angle can be calculated with the Merchants formula [14].

$$\phi_n^k = \frac{\pi}{4} - \frac{\beta_k}{2} + \frac{\gamma_n^k}{2} \tag{4}$$

The mean friction angle β_k can be defined by mean friction coefficient, and the mean friction coefficient may be a power function of the chip velocity, as shown in Fig. 4. The friction coefficient is given by:

$$f = f_0 V_c^p \tag{5}$$

where f_0 is constant, f is mean friction coefficient, while $p < 0$. The coefficients f_0 and p can be identified by the experimental data in orthogonal cutting.

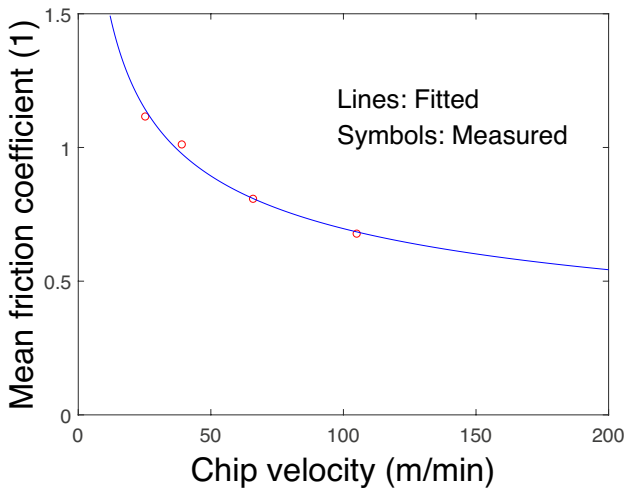

Fig. 4 The fitting curve of mean friction coefficient f with chip velocity V_c

3 Governing equations of the primary shear zone

Johnson–Cook model is used as flow stress model of workpiece material [27].

$$\tau^k = \frac{1}{\sqrt{3}}[A + B(\frac{\gamma^k}{\sqrt{3}})^{n}][1 + C\ln(\frac{\dot{\gamma}^k}{\dot{\gamma}_0})][1 - (\frac{T^k - T_r}{T_m - T_r})^{m}] \quad (6)$$

where τ^k, γ^k, $\dot{\gamma}^k$, and T^k are the shear stress, the shear strain, the shear strain rate, and the instantaneous temperature of the workpiece, respectively. $\dot{\gamma}_0$ is reference plastic strain rate, T_m is melting temperature of the workpiece material, and T_r is room temperature or initial workpiece temperature. A, B, C, m, and n is the material constants which can be identified through split Hopkinson bar (SPHB), the material coefficients of Johnson–Cook model are listed in Table 1.

The unequal division shear zone theory is used to predict the turning forces, as shown in Fig. 5. In this model, the strain, strain rate, and the temperature of discrete chip are calculated as follows [25]:

$$\dot{\gamma}^k = \begin{cases} \frac{\dot{\gamma}_m^k}{(k_u^k h)^q}(z_e^k)^q & z_e^k \in [0, k_u^k h] \\ \frac{\dot{\gamma}_m^k}{(1-k_u^k)^q h^q}(h - z_e^k)^q & z_e^k \in [k_u^k h, h] \end{cases} \quad (7)$$

Table 1 Johnson–Cook parameters of 304 stainless steel

A(MPa)	B(MPa)	C	n	$\dot{\gamma}_0(s^{-1})$	m
310	1000	0.07	0.65	1.00	1.00

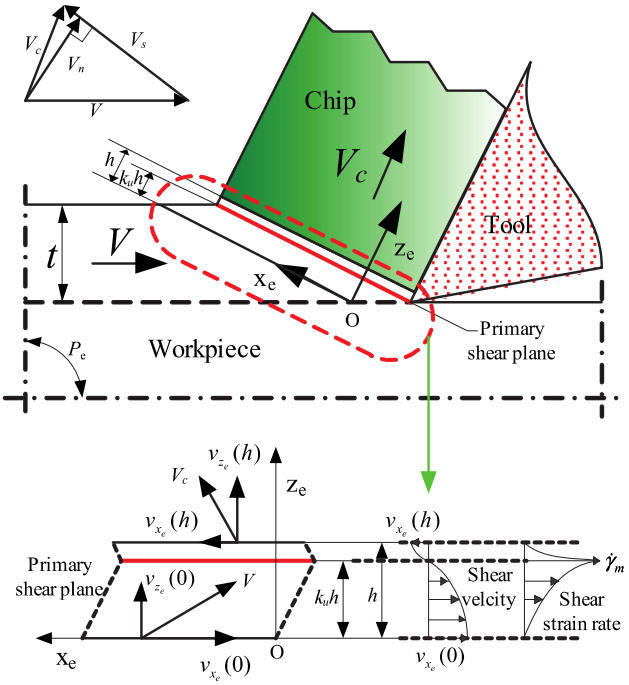

Fig. 5 The unequal division shear zone model

$$\gamma^k = \begin{cases} \frac{\dot{\gamma}_m^k \cos\eta_e^k}{(q+1)V\cos\lambda_s^k \sin\phi_n^k (k_u^k h)^q}(z_e^k)^{q+1} & z_e^k \in [0, k_u^k h] \\ -\frac{\dot{\gamma}_m^k \cos\eta_e^k}{(q+1)V\cos\lambda_s^k \sin\phi_n^k (1-k_u^k)^q h^q}(h - z_e^k)^{q+1} & \\ +\frac{\cos\gamma_n^k \cos\eta_e^k}{\cos(\phi_n^k - \gamma_n^k)\cos\eta_s^k \sin\phi_n^k} & z_e^k \in [k_u^k h, h] \end{cases} \quad (8)$$

where $\dot{\gamma}_m^k$ is the maximum strain rate, k_u^k is unequal division ratio, q is a parameter to characterize the non-uniform distribution of the tangential velocity in the primary shear zone, and h is the thickness of the primary shear zone; 0.025 mm is an acceptable approximation of h in reference by observing Shaw's research [28]. Besides, the boundary of the primary shear zone can be considered adiabatic so that the heat transfer equation can be expressed in the following form, and the chip temperature at the entry boundary is equal to the initial workpiece temperature.

$$k_u^k = \frac{\cos(\phi_n^k - \gamma_n^k)\cos\eta_s^k(\cos\phi_n^k \cos\eta_s^k + \tan\lambda_s^k \sin\eta_s^k)}{\cos\gamma_n^k} \quad (9)$$

$$\dot{\gamma}_m^k = \frac{(q+1)V\cos\lambda_s^k \cos\gamma_n^k}{h\cos\eta_s^k \cos(\phi_n^k - \gamma_n^k)} \quad (10)$$

$$\frac{dT^k}{dz_e^k} = \frac{\cos\eta_e^k}{\rho c V \sin\phi_n^k \cos\lambda_s^k} \mu\tau^k\dot{\gamma}^k \quad (11)$$

$$T|_{z_e^k=0} = T_w \tag{12}$$

Where ρ, c, and μ represent material density, heat capacity, and Taylor-Quinney coefficient, respectively. These values of 304 stainless steel are ρ=7900kg/m^3, c=400J/(kg·K) and μ=0.85, respectively. The material behavior and thermo-mechanical evolution in the primary shear zone are governed by Eqs. (6), (7), (8) and (11). Using the boundary conditions (12), the shear stress τ_s^k on the main shear plane can be calculated.

4 Cylindrical turning geometry and the cutting edge discretization

Considering the complexity of chip formation in turning, the majority of current research is based on the equivalent cutting edge method, i.e., a fictitious straight cutting edge is used to replace the real cutting edge, as shown in Fig. 6. When some studies need to know the local information about stress and temperature on the rake face, this method is very disadvantageous to the study of tool design and tool wear. Therefore, in order to obtain the component state of real cutting edge during chip formation, the cutting edge needs to be discretized.

In cylindrical turning, the modeling process is more complicated than the traditional oblique cutting with a single cutting edge on account for the existence of the tool rounded nose. In this paper, the discretization method of the cutting edge proposed by Molinnari and Moufki [22] is used to model the cylindrical turning process. The rounded edge is divided into finite straight cutting edge units. For each component edge unit, the expressions of component normal rake angle and inclination angle are derived by using geometric relationships. For the case of cylindrical turning, as shown in Fig. 7. The cutting conditions to be given are cutting velocity V, feed rate f_r, cutting depth a_p, and tool geometric parameters (the main cutting edge angle κ_r, inclination angle λ_s, normal rake angle γ_n and nose radius r_n); the tool geometry is defined by six planes (P_r, P_s, P_n, P_o, P_f, and P_p) to determine the spatial position of the cutting edge. Figure 8 illustrates the discrete process of tool nose in cylindrical turning.

On the reference plane P_r, the cutting edge can be discretized into K+2 parts of the straight cutting edge section by the index k ($0 \le k \le$ K + 1). The tool nose is discretized into K+1 straight cutting edge units, and the chip thickness corresponding to each component edge unit is variable as shown in Fig. 8. In the turning process, the rounded edge in contact with the workpiece can be divided into two parts by the angles ϕ_s and ϕ_a respectively. ϕ_{st} and ϕ_{ex} are the entry and exit angles in the first part (see Fig. 8). The first part (for the interval angle of ϕ_s) can be subdivided into K cutting edge units which are identified as k ($1 \le k \le$ K), and $\Delta\phi$ is taken as the increment angle. The second part is also considered as a single unit with the index k = K + 1. Figure 8 shows an

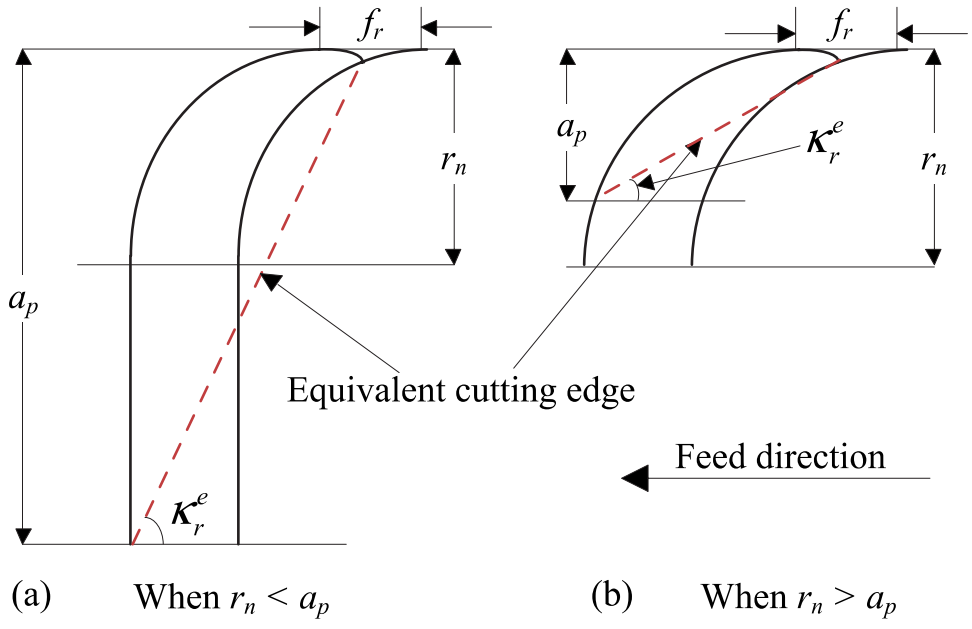

Fig. 6 The equivalent cutting edge method

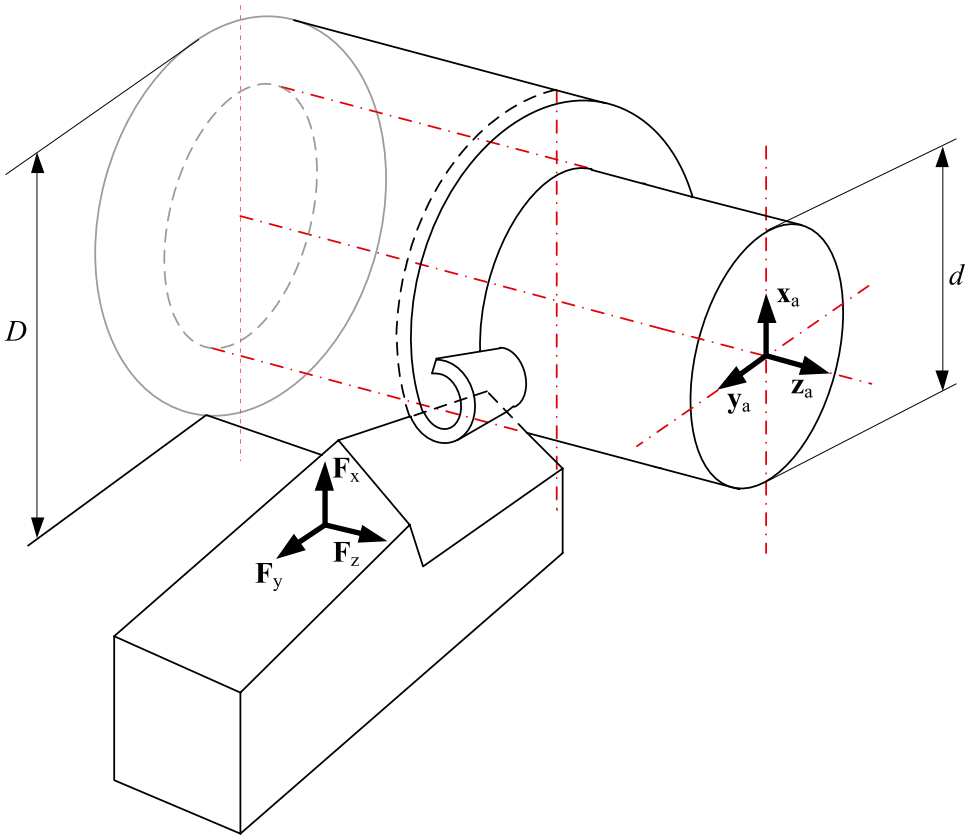

Fig. 7 The Geometric model of cylindrical turning

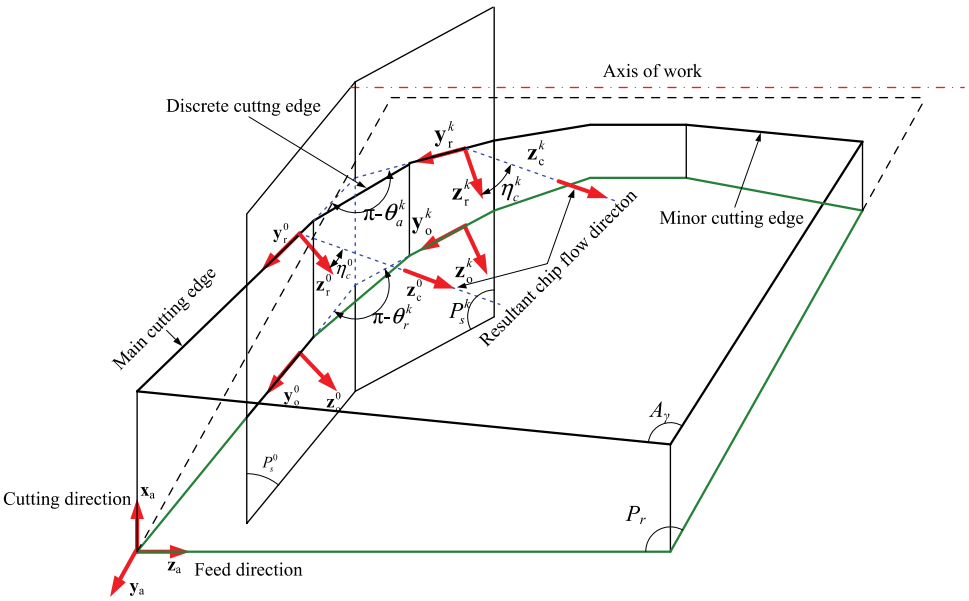

Fig. 8 The cutting edge discretization of the engaged part in the rake face

example of discretization for K = 3, which corresponds to the projection of a discrete cutting edge on the reference plane. According to the geometric relationship, the following equations of these angles can be obtained:

$$\phi_{st} = \begin{cases} \arcsin((r_n - a_p)/r_n) & a_p < r_n(1-\cos\kappa_r) \\ \pi/2 - \kappa_r & a_p \geq r_n(1-\cos\kappa_r) \end{cases} \tag{13}$$

$$\phi_{ex} = \pi/2 - \arcsin(0.5 f_r/r_n) \tag{14}$$

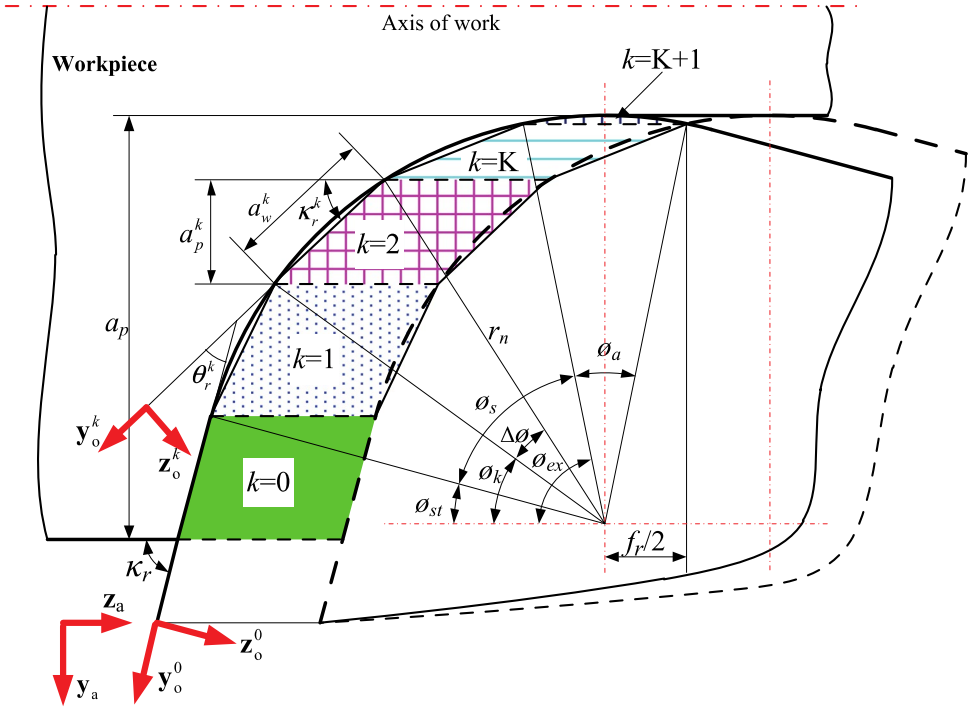

Fig. 9 Projection of discrete cutting edge on reference plane

$$\phi_s = \phi_{ex} - \phi_{st} \tag{15}$$

$$\Delta\phi = \phi_s/\mathrm{K} \tag{16}$$

$$\phi_a = 2\arcsin(0.5 f_r/r_n) \tag{17}$$

For the rounded edge, the geometric description of the discrete cutting edge is mainly defined by the planes P_r,P_s^0,P_n^0,P_s^k, and P_n^k, as shown in Fig. 8. P_s^0 and P_n^0 correspond to the cutting plane and normal plane of the main cutting edge ($k=0$). P_s^k is defined as containing the kth component edge and being perpendicular to P_r. P_n^k is normal to the kth component edge. θ_r^k is the angle between the planes P_s^0 and P_s^k measured in the plane P_r, θ_a^k is the angle between the main cutting edge ($k=0$) and the kth component edge ($1 \le k \le \mathrm{K}$) measured in the tool rake face (see Fig. 8). As shown in Fig. 9, the component parameters ϕ_k,κ_r^k,φ_r^k ,θ_r^k,a_w^k, and t_k in the reference plane P_r can be obtained as below:

$$\phi_k = \phi_{st} + (k-1)\Delta\phi \tag{18}$$

$$\kappa_r^k = \pi/2 - \phi_k - \Delta\phi/2 \tag{19}$$

$$\varphi_r^k = \pi/2 - \kappa_r^k \tag{20}$$

$$\theta_r^k = \kappa_r - \kappa_r^k = \phi_k - \pi/2 + \kappa_r + \Delta\phi/2 \tag{21}$$

$$a_w^k = 2 r_n \sin(\Delta\phi/2) \tag{22}$$

$$t_k = f_r \sin(\kappa_r^k) \tag{23}$$

where ϕ_k, κ_r^k, φ_r^k, a_w^k, and t_k represent, respectively, the angular position, the component cutting edge angle, the component lead angle, the component cutting width, and the component cutting thickness corresponding to the kth component cutting edge. The following relations can be obtained for the main cutting edge ($k=0$):

$$\begin{cases} \theta_r^0 = 0 \\ a_w^0 = \begin{cases} 0 & a_p < r_n(1-\cos\kappa_r) \\ (a_p - r_n(1-\cos\kappa_r^0))/\sin\kappa_r^0 & a_p \ge r_n(1-\cos\kappa_r) \end{cases} \quad k=0 \\ t_0 = f_r \sin(\kappa_r^0) \end{cases} \tag{24}$$

The chip load A^k of the kth ($0 \le k \le \mathrm{K}$) component edge is defined as the undeformed chip area. For the chip load $A^{\mathrm{K}+1}$ of the $k=\mathrm{K}+1$ component edge, the following relationship can be obtained.

$$A^k = a_w^k t_k \qquad 0 \le k < \mathrm{K} \tag{25}$$

$$A^{\mathrm{K}+1} = r_n^2 \arcsin(0.5 f_r/r_n) - 0.5 f_r \sqrt{r_n^2 - (f_r)^2/4} \tag{26}$$

The relationship between the discrete cutting edge on the rake face and its projection on P_r is processed by coordinate transformation. The component cutting conditions corresponding to each component cutting edge, that is, the component cutting angles (cutting edge angle, inclination angle, normal rake angle) and the component undeformed chip area,

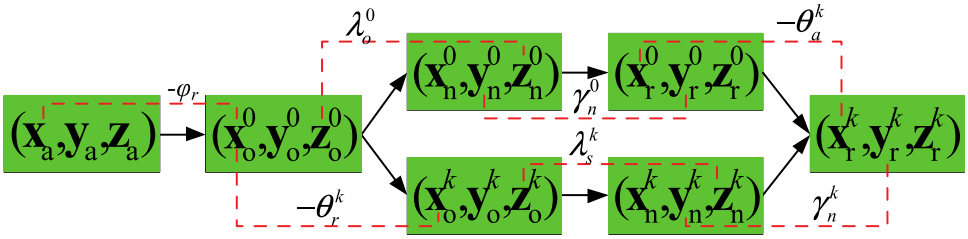

Fig. 10 Coordinate transformation relationship in the discrete process of turning tool

are also determined. In the rake face. The projection of y_r^k on the reference plane P_r is oriented by the unit vector y_o^k; y_r^k is the vector along the kth component edge and is contained in the P_s^k as shown in Fig. 9. To calculate the angles θ_a^k, λ_s^k, and γ_n^k, a set of frames is introduced. These frames can be related by rotation transformation, as shown in Fig. 10. Based on the relationship of the coordinate systems shown in Fig. 10, the following expression can be obtained:

$$\mathbf{R}(x_r^0, -\theta_a^k) \cdot \mathbf{R}(y_n^0, \gamma_n^0) \cdot \mathbf{R}(z_o^0, \lambda_s^0) = \mathbf{R}(y_n^k, \gamma_n^k) \cdot \mathbf{R}(z_o^k, \lambda_s^k) \cdot \mathbf{R}(x_o^0, -\theta_r^k) \tag{27}$$

Therefore, by considering Eq. (27) and after some algebraic manipulation, θ_r^k corresponding to the projection of θ_a^k in the reference plane P_r is obtained:

$$\tan\ \theta_a^k = \frac{\cos\ \lambda_s^0 \tan\ \theta_r^k}{\cos\ \gamma_n^0 - \tan\ \theta_r^k \sin\ \gamma_n^0 \sin\ \lambda_s^0} \tag{28}$$

The component inclination angle λ_s^k and the component normal rake angle γ_n^k for the kth component edge are measured in P_s^k and P_n^k, respectively. For the main cutting edge ($k=0$), the cutting angles are given by $\lambda_s^0 = \lambda_s$ and $\gamma_n^0 = \gamma_n$. The angles λ_s^k and γ_n^k, for $1 \le k \le \mathrm{K}+1$, are determined from the following relationships by Eq. (27).

$$\sin\ \lambda_s^k = \cos\ \theta_a^k \sin\ \lambda_s^0 - \sin\ \theta_a^k \sin\ \gamma_n^0 \cos\ \lambda_s^0 \tag{29}$$

$$\sin\ \gamma_n^k = \cos\ \theta_r^k \sin\ \gamma_n^0 + \sin\ \theta_r^k \sin\ \lambda_s^0 \cos\ \gamma_n^0 \tag{30}$$

The component cutting edge geometry can be characterized by these angles κ_r^k, γ_n^k, λ_s^k, θ_r^k, and θ_a^k.

5 Cutting forces model of cylindrical turning

5.1 Component equilibrium of the discrete chip unit

For the improved oblique cutting model, the shear force F_s^k and normal force F_{ns}^k exerted by the workpiece on the kth chip unit can be expressed as:

$$\mathbf{F}_k = -F_s^k \mathbf{x}_s^k + F_{ns}^k \mathbf{z}_s^k \tag{31}$$

The component force balance acting on the kth chip unit can be expressed in the form of a vector:

$$-F_s^k \mathbf{x}_s^k + F_{ns}^k \mathbf{z}_s^k + F_{nc}^k \mathbf{x}_c - F_{fc}^k \mathbf{z}_c + F_{mc}^k \mathbf{y}_c = 0 \tag{32}$$

Equation (32) can be transformed into the component equations in the coordinate system ($\boldsymbol{x}^k$, $\boldsymbol{y}^k$, $\boldsymbol{z}^k$). The following expressions were deduced by Moufki and Molinari [26].

$$\begin{cases} F_{nc}^k(\cos(\phi_n^k - \gamma_n^k) - \tan\beta_k \sin(\phi_n^k - \gamma_n^k)\cos\eta_c^k) - F_{mc}^k \sin(\phi_n^k - \gamma_n^k)\sin\eta_c^k - F_s^k \cos\eta_s^k = 0 \\ F_{nc}^k \tan\beta_k \sin\eta_c^k - F_{mc}^k \cos\eta_c^k - F_s^k \sin\eta_s^k = 0 \\ F_{nc}^k(\sin(\phi_n^k - \gamma_n^k) + \tan\beta_k \cos(\phi_n^k - \gamma_n^k)\cos\eta_c^k) + F_{mc}^k \cos(\phi_n^k - \gamma_n^k)\sin\eta_c^k - F_{ns}^k = 0 \end{cases} \tag{33}$$

Equation (33) is an algebraic equation which can be solved by combing with F_s^k. Meanwhile, the unknown forces F_{nc}^k, F_{mc}^k, and F_{ns}^k can be determined. The shearing force F_s^k is given by:

$$F_s^k = \frac{\tau_s^k}{\cos\ \lambda_s^k \sin\ \phi_n^k} A_k \tag{34}$$

where τ_s^k is the shear stress on the main shear plane of the primary shear zone; it can be obtained from the unequal division shear zone theory.

5.2 Resultant chip equilibrium and cutting forces.

In order to determine the value of the main chip flow angle η_c^0, the resultant force balance equation acting on the entire chip can be simplified as:

$$\sum_{k=0}^{\mathrm{K}+1} (-F_s^k \mathbf{x}_s^k + F_{ns}^k \mathbf{z}_s^k + F_{nc}^k \mathbf{x}_c - F_{fc}^k \mathbf{z}_c) = 0 \tag{35}$$

Through combining Eqs. (32) and (35), the implicit Eq. (36) can be obtained, and the main chip flow angle can be obtained by Eqs. (36) and (32). In the resultant chip balance, the sum of F_{mc}^k is equal to zero for the interaction force F_{mc}^k between discrete chip units.

$$\sum_{k=0}^{\mathrm{K}+1} F_{mc}^k = 0 \tag{36}$$

Because the variables η_e^k, η_s^k, ϕ_n^k, β_k, and F_{mc}^k all depend on the main chip flow angle η_c^0, numerical iteration is applied to

obtain their values. The main chip flow angle η_c^0 is determined by Eq. (36), it considers the influence of material properties of workpiece, tool geometry, and cutting parameters. Adibi-Sedeh et al. [29] considered the effects of the nose-rounded radius and the cutting angle on the chip flow direction when the main cutting edge angle is not equal to zero for the traditionally defined equivalent cutting edge.

For the improved oblique cutting model of the kth component edge, in Fig. 3, the resultant force $\mathbf{F}_k$ is expressed as the ($\mathbf{x}_o^k$, $\mathbf{y}_o^k$,$\mathbf{z}_o^k$) components of F_c^k (cutting force), F_d^k (back force), and F_f^k (feed force).

$$\mathbf{F}_k = -F_c^k\mathbf{x}_o^k - F_d^k\mathbf{y}_o^k + F_f^k\mathbf{z}_o^k \tag{37}$$

$$\begin{pmatrix} F_c^k \\ F_d^k \\ F_f^k \end{pmatrix} = \begin{pmatrix} cos\eta_s^k\ cos\phi_n^k\ cos\lambda_s^k + sin\eta_s^k\ sin\lambda_s^k\ sin\phi_n^k\ cos\lambda_s^k \\ cos\eta_s^k\ cos\phi_n^k\ sin\lambda_s^k - sin\eta_s^k\ cos\lambda_s^k\ sin\phi_n^k\ sin\lambda_s^k \\ -cos\eta_s^k sin\phi_n^k \qquad\qquad cos\phi_n^k \end{pmatrix} \begin{pmatrix} F_s^k \\ F_{ns}^k \end{pmatrix} \tag{38}$$

These force components can then be transformed to the frame ($\mathbf{x}_a$, $\mathbf{y}_a$, $\mathbf{z}_a$) by:

$$\begin{pmatrix} F_x^k \\ F_y^k \\ F_z^k \end{pmatrix} = \begin{pmatrix} 1 & 0 & 0 \\ 0 & -\cos\varphi_r^k & \sin\varphi_r^k \\ 0 & \sin\varphi_r^k & \cos\varphi_r^k \end{pmatrix} \begin{pmatrix} F_c^k \\ F_d^k \\ F_f^k \end{pmatrix} \tag{39}$$

where F_x^k is the tangential force, F_y^k is radial force, and F_z^k is the longitudinal force as shown in Fig. 2. The algorithm to calculate cutting forces for cylindrical turning is as follows in Fig. 11.

At the beginning, the component cutting angles can be calculated by giving an initial value of η_c^0, These output parameters such as strain, strain rate, stress, and temperature distributions in the primary shear zone for each chip unit can be computed by numerical iterative method. If $\sum_{k=0}^{K+1} F_{mc}^k$ is not equal to zero, a new estimated value of η_c^0 will be obtained

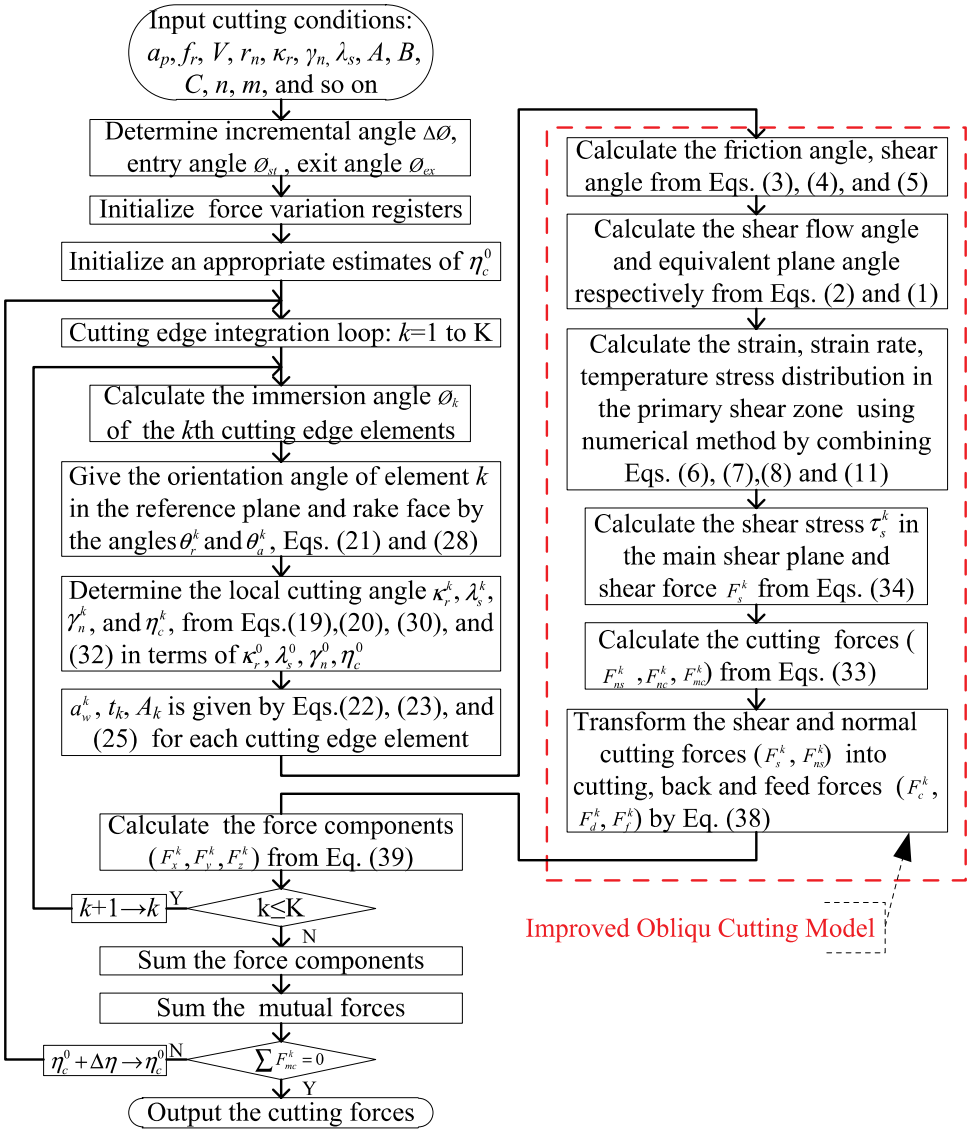

Fig. 11 Flow chart for the improved oblique cutting model applied to cylindrical turning

by adding an increment $\Delta\eta$. The computation will stop until the iteration requirement is satisfied. Conclusively, the component cutting force (F_x^k, F_y^k, F_z^k) of the kth cutting edge unit is deduced by Eqs. (38) and (39); F_{mc} can be determined by Eq. (36). All steps of calculations were performed programmatically by MATLAB software.

6 Experimental validation and analysis

In order to validate the proposed method above, a series of turning experiments for 304 stainless steel were conducted without cutting fluid in Mazak lathe. The cutting forces were measured by Kisler Dynamometer (6275A); the force signals that pass through the charge amplifier (5070A) was addressed by the Dynoware software, as shown in Fig. 12. The experiment was carried out in three cases:

- The influence of cutting depth a_p, feed rate f_r, and cutting velocity V on turning forces was analysed with different cutting parameters.
- The influence of the tool nose radius r_n on turning forces was analysed with different tool insert.
- The influence of the main cutting edge angle κ_r on turning forces was analysed with different toolholder.

6.1 Effects of cutting conditions

The experiment used SNMG120408-MR2025 insert and DSBNR2525M12 holder of Sandvik to study the influence of cutting parameters on turning forces of 304 stainless steel. The geometry parameters of the insert and the cutting conditions are shown in Tables 2 and 3, respectively. Specifically, there were three procedures in the experiment to obtain the reliable results, namely, the experiment with the same cutting parameters was repeated twice; the measurement interval time of the cutting process is more than 10 s, and the insert was replaced by a new one after each cutting test with the same cutting parameters.

Table 2 Geometry parameters of tool insert

The main cutting edge angle(κ_r)	Inclination angle(λ_s)	Normal Rake angle(γ_n)	Radius of tool nose(r_n)
75°	−6°	0°	0.8 mm

Table 3 Cylindrical turning conditions of 304 stainless steel

Feed rate f_r(mm/r)	Cutting depth a_p(mm)	Cutting velocity V(m/min)
0.075	0.5	62
0.1	1	90
0.15	1.5	132
0.2	2.0	188

In Fig. 13, it can be seen that the cutting force increases approximately linearly with the increase of cutting depth. When the cutting depth is very small, the change of cutting force shows obvious nonlinearity. The reason is that the straight main cutting edge plays a leading role in the cutting process when the cutting width a_w ($a_w = a_p/\sin(\kappa_r)$) increases in a positive proportion with the cutting depth increases. Furthermore, when the cutting depth is close to the nose radius, the influence of the nose radius on the cutting force must be considered. At this time, the nonlinear variation can only be measured in a more stable environment with precise equipment.

As shown in Fig. 14, the cutting force also shows a linear trend with increasing feed rate, which is different from the effect of cutting depth on cutting force. This is because the chip thickness t ($t = f_r\sin(\kappa_r)$) has been increasing in a positive proportion with the increase of feed rate. However, with the increase of feed speed, the increase of temperature will lead to the decrease of friction coefficient and cutting force in the turning process. Considering the positive and negative effects, the influence of feed rate on cutting force should be nonlinear. At the same time, it can be found from Figs. 14a

Fig. 12 The experiments of cutting forces in cylindrical turning of 304 stainless steel

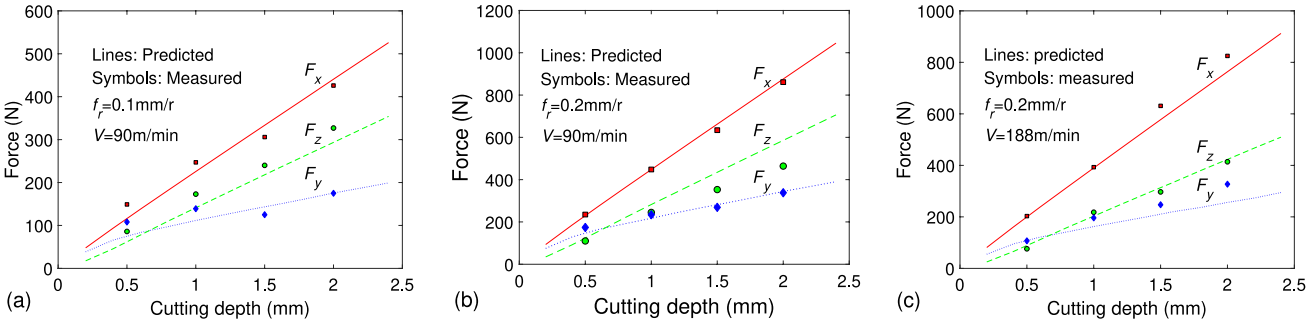

Fig. 13 The effect of cutting depth a_p on turning forces

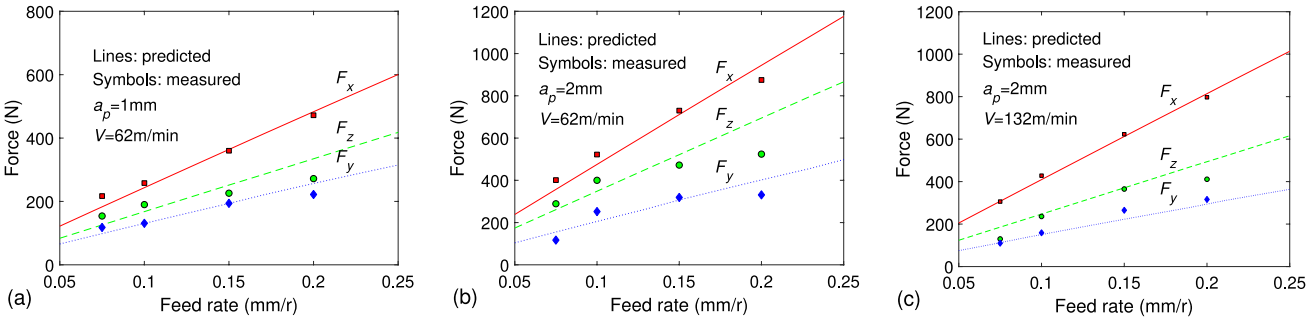

Fig. 14 The effect of feed rate f_r on turning force

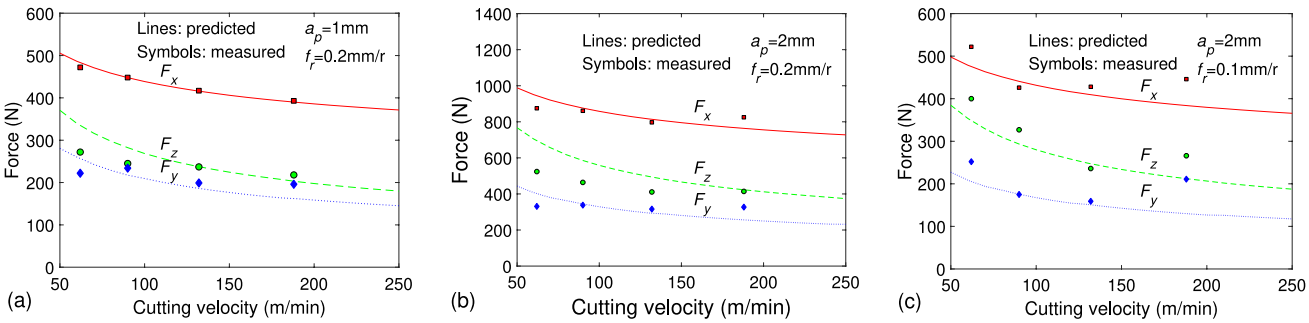

Fig. 15 The effect of cutting speed V on turning force

and b that the cutting force increase is slow with the increase in feed rate when the cutting velocity is very high.

For the 304 stainless steels, the nonlinear effect of cutting velocity on turning force is shown in Fig. 15. It can be seen that the cutting force decreases with the increase of cutting velocity in Fig. 15; the variation trend of cutting forces is consistent with the experimental results of Young et al. [10]. and Arsecularate et al. [30]. This is due to the fact that the deformation coefficient and friction coefficient decrease with the cutting velocity increases. It should be noted that the tool-chip friction is mainly caused by high temperature, high pressure, and high chip velocity. In cylindrical turning, the friction coefficient of each discrete chip unit will change, the average tool-chip temperature decreases with the cutting velocity increases, which will lead to the decrease of average tool-chip friction coefficient and cutting force. Meanwhile, it can be seen in Fig. 15 that the changing ratio of cutting force is obviously slow when cutting velocity is very low.

6.2 Effects of the main cutting edge angle

The cutting experiments of 304 stainless steel with three kinds of the main cutting edge angle were carried out. Table 4 illustrates the geometric parameters of the tool, and normal rake angle γ_n is approximately regarded as 0°,

Table 4 The tool geometric parameters

Tool insert	Tool holder	The main cutting edge angle κ_r
SNMG 12 04 08-MM 2025	DSDNN 2525 M12	45°
SNMG 12 04 08-MM 2025	DSBNR 2525 M12	75°
SNMG 12 04 08-MM 2025	PTGNR 2525 M16	90°

inclination angle λ_s is − 6°, and nose radius r_n is 0.8 mm. The predicted values of the proposed model and the experimental results are shown in Fig. 16; the main cutting edge angle κ_r is investigated in the range of 30° to 90°. It can be found from Fig. 16 that the influence of the main cutting edge angle is approximately linear. As the main cutting edge angle increases, F_x and F_z are increasing, F_y is decreasing, and this trend is consistent with the experimental results of Young et al. [10]. However, F_x basically remains constant with the increase of the main cutting edge angle. Although the incensement of the main cutting edge angle will result in a decrease in the engaged length in cutting, the area A ($A = f_r a_p$) of the undeformed chip which mainly determines the cutting force not depend on the tool main cutting edge angle. It can be seen in Fig. 16 that F_x is increased significantly when the main cutting edge angle increases to the range between 60 and 90°. It can generally be considered that the main cutting edge angle mainly affects the cutting force through the cutting thickness. With the increase of κ_r, the contact length of the tool rounded edge will also increase (at this time, the non-free cutting effect will be more significant). When the cutting area is constant, the cutting thickness increases with the increase of the main cutting edge angle. As a result, the deformation of chip formation will become large, which will lead to the increase of F_x. Nevertheless, the cutting thicknesses of the discrete chip units for tool nose part decreases in order as shown in Fig. 16, and they are smaller than the cutting thickness of the main cutting edge. When the cutting area is constant and the main cutting edge angle is increased, the cutting thickness will increase. The influence of the main cutting edge angle on F_z and F_y is mainly through the projection components of the resultant cutting force in the Z and Y directions. Therefore, F_z will decrease and F_y will increase as the main cutting edge angle increases.

6.3 Effects of the tool nose radius

The effect of four kinds of the tool nose radius on turning force of 304 stainless steel was studied. The rounded edge parameters are presented in Table 5. Figure 17 illustrates the predicted variation of turning force with the nose radius and the experimental results. In the experiments, the main cutting edge is not involved in cutting process ($a_p < r_n(1\text{-}\cos(\kappa_r))$. It can be seen in Fig. 17a that F_x is basically a constant, which may be because the total undeformed chip area A is nearly independent of the nose radius and only related to feed rate and cutting depth. The predicted curve in Fig. 17 shows an increase of F_y and a decrease of F_z with the increase of the nose radius. The

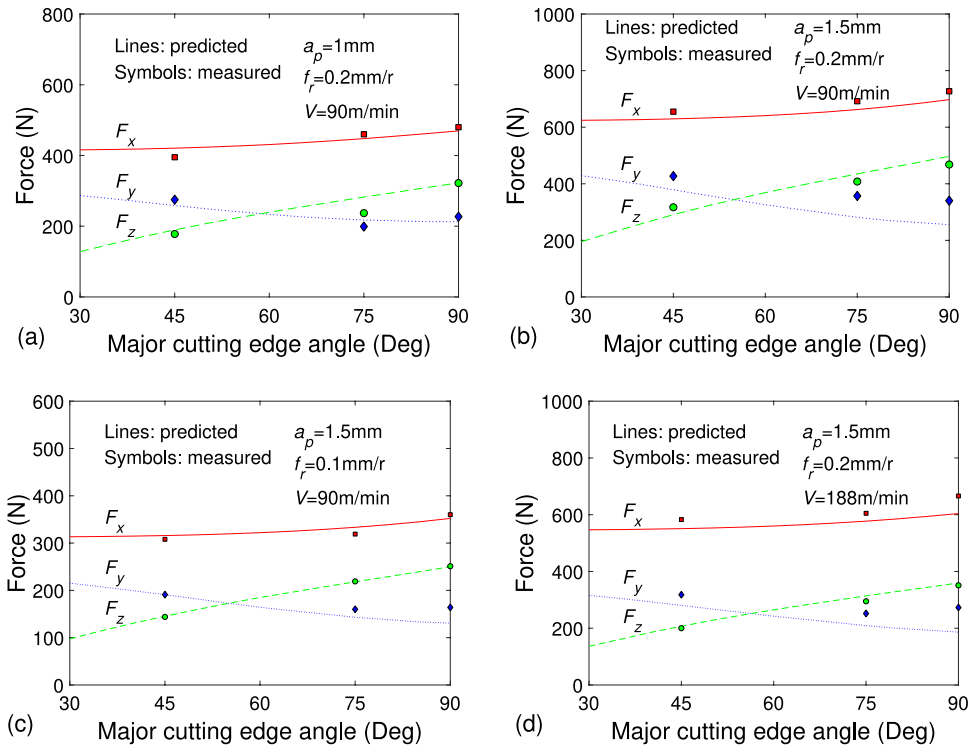

Fig. 16 The effect of the main cutting edge angle κ_r on turning force

Table 5 The tool rounded edge parameters

Tool insert	Tool holder	Tool nose radius
SNMG 12 04 04-MF 2015	DSBNR 2525 M12	0.4 mm
SNMG 12 04 08-MM 2025	DSBNR 2525 M12	0.8 mm
SNMG 12 04 12-MM 2025	DSBNR 2525 M12	1.2 mm
SNMG 12 04 16-MM 2025	DSBNR 2525 M12	1.6 mm

experimental results of 304 stainless steel are also basically consistent with the predicted law, which is also consistent with the experimental results of Young [10] and Arsecularatne et al. [30]. According to the previous discussion, F_z will increase with the increase of the main cutting edge angle and decrease with the increase of η_c^0; the change law of F_y is opposite. However, when the main cutting edge is involved in cutting ($a_p > r_n(1-\cos(\kappa_r))$), as shown in Fig. 17b and c. When the cutting depth a_p and feed rate f_r are constant, the tool nose radius length and cutting width increase with the increase of the main cutting edge angle. Conversely, the cutting thickness and the tool component cutting edge angle of the discrete edge units will decrease; these lead to the increase of cutting deformation and cutting force. It has a greater influence on F_y than on F_x as shown in Fig. 17.

7 Conclusion

This paper extended the previous work for the traditional oblique cutting model to non-free turning with a rounded edge. The main conclusions can be summarized as follows:

- The improved oblique cutting model considers the condition that the main cutting edge angle is unequal to be 90° and the tool nose has a rounded edge.
- Through applying the coordinate transformation method, the geometry relations for the non-free turning are analysed. The unequal division shear zone theory in orthogonal cutting is used in oblique cutting modeling.
- The tool rounded edge was discretized into small oblique cutting edges characterized by component cutting angles. For every engaged cutting chip unit, the cutting forces in different directions are obtained during oblique cutting. The effects of tool geometrical parameters and workpiece material properties on the cutting force are considered as their coupling interaction.

A MATLAB-based program has been given to facilitate the application of the analytical model for cutting forces. The experiments with three types of cutting conditions have been conducted to validate the prediction model and the deviation between the predicted results and experiment data is within an acceptable range. The proposed models have also been used to investigate the effects of cutting conditions and tool angles on the cutting forces. This quantitative information is helpful in selecting the appropriate cutting parameters and optimization of cutting edge geometry. It should be noted that the above description law of the influence of the machining parameters on the turning forces has appeared in many literatures, but most are obtained by curve fitting from the experimental results. The significance of

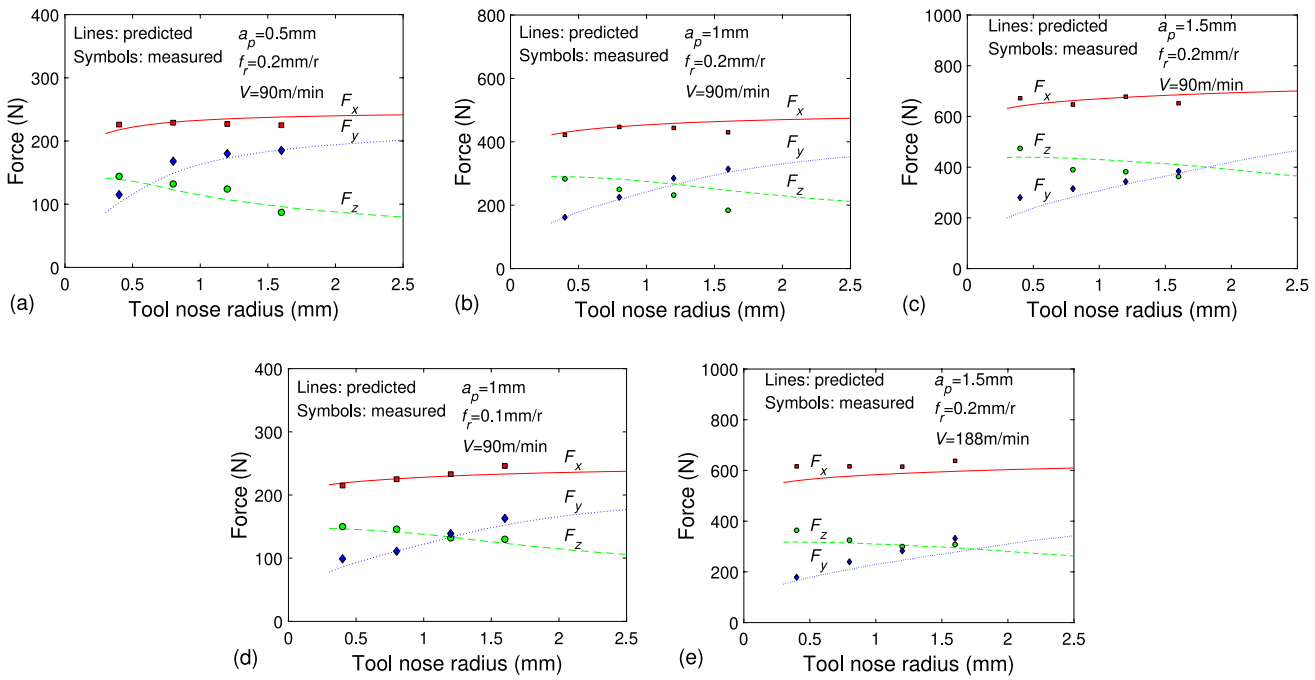

Fig. 17 The effect of tool nose radius r_n on turning force

this paper lies in proposing a new analytical model to predict the trend, and these methods are mutually verified.

Author contribution Binglin Li: Conceptualization, methodology, formal analysis, validation. Rui Zhang: writing—original draft, review, and editing.

Data availability The data and materials sets supporting the results of this article are included within the article.

Code availability Not applicable.

Declarations

Ethics approval Not applicable.

Consent to participate Not applicable.

Consent for publication All of the authors have informed us of their consent to the publication of the paper.

Competing interests The authors declare no competing interests.

References

1. Venkatarao K, Harish BB, Umasai VPV (2019) A study on effect of dead metal zone on tool vibration, cutting and thrust forces in micro milling of Inconel 718. J All Comp 793:343–351
2. Harish BB, Venkatarao K, Satishben B (2021) Modeling and optimization of dead metal zone to reduce cutting forces in micro-milling of hardened AISI D2 steel. J Braz Soc Mech Sci Eng 43:142
3. Parakkal G, Zhu RX, Kappor SG, DeVor RE (2002) Modeling of turning process cutting forces for grooved tools. Int J Mach Tool Manufact 1:179–191
4. Kone F, Czarnotab C, Haddaga B, Nouari M (2013) Modeling of velocity-dependent chip flow angle and experimental analysis when machining 304L austenitic stainless steel with groove coated-carbide tool. J Mater Process Technol 213:1166–1178
5. Venkatarao K (2019) Power consumption optimization strategy in micro ball-end milling of D2 steel via TLBO coupled with 3D FEM simulation. Measur 132:68–78
6. Venkatarao K, Umasai VPV, Satishben B (2022) A comparative study on cutting forces and power consumption in plain and ultrasonic vibration helical milling of AISI 1020 steel. Proc Inst Mech Eng Part B 236(13):1726–1737
7. Colwell LV (1954) Predicting the angle of chip flow for single-point cutting tools. Trans ASME 76:199–204
8. Hu RS, Mathew P, Oxley PLB, Young HT (1986) Allowing for end cutting edge effects in predicting forces in bar turning with oblique machining conditions. Proc Inst Mech Eng 200:89–99
9. Kushima KO, Minato K (1987) On the behaviors of chip in steel cutting. JSME Int J 2:58–64
10. Young HT, Mathew P, Oxley PLB (1987) Allowing for nose radius effects in predicting the chip flow direction and cutting forces in bar turning. Proc Inst Mech Eng 201:213–226
11. Wang J, Mathew P (1995) Development of a general tool model for turning operations based on a variable flow stress theory. Int J Mach Tool Manufact 1:71–90
12. Endres WJ, Waldorf DJ (1994) The importance of considering size effect along the cutting edge in predicting the effective lead angle for turning. North Am Manuf Res Conf 22:65–72
13. Khlifi H, Abdellaoui L, Bouzid SW (2019) An equivalent geometry model for turning tool with nose and edge radii. Int J Adv Manuf Technol 103:4233–4251
14. Merchant E (1945) Mechanics of the metal cutting process. J Appl Phys 16:267–275
15. Oxley PLB, Young H (1989) The mechanics of machining: an analytical approach to assessing machinability. Ellis Horwood Publisher, New York
16. Li BL, Wang XL, Hu YJ, Li CG (2011) Analytical prediction of cutting forces in orthogonal cutting using unequal division shear zone model. Int J Adv Manuf Technol 54:431–443
17. Redetzky M, Balaji AK, Jawahir IS (1999) Predictive modeling of cutting forces and chip flow angle in machining with nose radius tools. In: Proceedings 2nd CIRP International Workshop on Modeling of Machining Operations, Nantes France, July 3-5, pp 160–180
18. Hagiwara M, Chen S, Jawahir IS (2009) A hybrid predictive model and validation for chip flow incontour finish turning operations with coated grooved tools. J. Mater Process Technol 209:1417–1427
19. Armarego EJA, Samaranayake P (1999) Performance prediction models for turning with rounded corner plane faced lathe tool theoretical development. Mach Sci Technol 3:143–172
20. Storch B, Zawada-Tomkiewicz A (2012) Distribution of unit forces on the tool nose rounding in the case of constrained turning. Int J Mach Tool Manufact 57:1–9
21. Fang N (1998) An improved model for oblique cutting and its application to chip-control research. J Mater Process Technol 79:79–85
22. Molinari A, Moufki A (2005) A new thermomechanical model of cutting applied to turning operations. Part I. Theory Int J Mach Tool Manufact 45:166–180
23. Budak A, Ozlu E (2008) Development of a thermomechanical cutting process model for machining process simulations. CIRP Ann-Manuf Technol 57:97–100
24. Abdellaoui L, Khlifi H, Bouzid SW, Hamdi H (2020) Tool nose radius effects in turning process. Int J Mach Sci Technol 25:1–30
25. Li BL, Hu YJ, Wang XL, Li CG, Li XX (2011) An analytical model of oblique cutting with application to end milling. Int J Mach Sci Technol 15:453–484
26. Moufki A, Molinari A (2005) A new thermomechanical model of cutting applied to turning operations. Part II. Parametric study. Theory Int J Mach Tool Manufact 45:181–193
27. Johnson GR, Cook WH (1985) Fracture characteristics of three metals subjected to various strains, strain rates, temperatures and pressures. Eng Fract Mech 21:31–78
28. Shaw MC (2005) Metal cutting principles, Second published. Oxford University Press, Oxford, UK
29. Adibi-Sedeh AH, Madhavan V, Bahr B (2003) Upper bound analysis of oblique cutting: Improved method of calculating the friction area. Int J Mach Tool Manufact 43:485–492
30. Arsecularatne JA, Mathew P, Oxley PLB (1995) Prediction of chip flow direction and cutting forces in oblique machining with nose radius tools. Proc Inst Mech Eng 209:305–315